PHYSICAL REVIEW APPLIED **13,** 054073 (2020)

Direct Probe of Room-Temperature Quantum-Tunneling Processes in Type-II Heterostructures Using Terahertz Emission Spectroscopy

Markus Stein,[1,*] Christian Fuchs,[1] Wolfgang Stolz,[1] Daniel M. Mittleman,[2] and Martin Koch[1]

[1] *Department of Physics and Material Sciences Center, Philipps-Universität Marburg, Renthof 5, 35032 Marburg, Germany*

[2] *School of Engineering, Brown University, 184 Hope Street, Providence, Rhode Island 02912, USA*

(Received 17 August 2019; revised manuscript received 28 October 2019; accepted 27 April 2020; published 28 May 2020)

Charge-carrier-transport phenomena on nanoscopic length and ultrashort timescales are of great interest for a multitude of ultrafast dynamic processes occurring in chemical reactions as well as modern devices such as solar cells or transistors. However, the investigation of such ultrashort current pulses is very challenging and mostly based on indirect methods such as spectroscopic changes induced by the charge transport. Here we monitor the short current pulse generated by the dissipative tunneling of charge carriers through a barrier between two adjacent quantum wells via its radiated legacy in the terahertz frequency range. By examining quantum structures with intermediate barriers of different thickness, we demonstrate that the spectrum of the emitted radiation is a direct measurement of the charge-transfer dynamics associated with the tunneling process. Our findings indicate that these incoherent tunnel currents do not start instantaneously but build up on a timescale of approximately 170 fs.

DOI: 10.1103/PhysRevApplied.13.054073

I. INTRODUCTION

Charge-transport phenomena on ultrashort length scales that are dominated by quantum mechanics are of tremendous interest for a variety of dynamic systems. They are key for a fundamental understanding of ultrafast processes and are, due to the ongoing miniaturization of systems, also of great relevance for a large number of modern electronic and optical devices. For such devices, in particular ultrafast tunnel phenomena through internal interfaces on nanometer or subnanometer length scales are of growing interest and often limit their miniaturization or performance. As a prototype example, a quantum-cascade laser uses a complicated nanostructure of quantum wells and barriers to engineer a specific band structure, exploiting rapid charge-tunneling processes to achieve a population inversion between conduction-band sublevels [1,2]. In an effort to clarify the ultrafast dynamics associated with such processes, researchers have investigated a variety of different artificial quantum structures using a vast scope of experimental techniques, including various types of pump-probe measurements [3–6] and time-resolved photoluminescence [7–9]. Yet, these methods are only indirect probes of the process of charge tunneling through a barrier. Instead of measuring the current associated with the charge transfer, the photoluminescence or the differential absorption, which are sensitive to changes in the occupation of the relevant quantum states, is measured. As such, these measurements are also influenced by complex many-body effects such as Coulomb screening, relaxation and scattering processes, or coherent phenomena that are superimposed on the signatures of the charge transfer [10–12]. In contrast, terahertz emission spectroscopy is a direct probe with an unambiguous origin: an ultrafast current induced by a femtosecond optical pulse gives rise to a terahertz electromagnetic signal, whose origin is therefore solely due to the transient current associated with the charge-transfer process. As a result, terahertz emission has become a valuable tool for spectroscopic studies of optically induced charge motion in many different material systems [13–16]. In our case, terahertz emission spectroscopy is well suited for probing the real-space motion of charges as they tunnel through barriers. The technique has been exploited as the most-direct approach to observe coherent wave-packet motion in biased quantum-well structures [17,18]. In these earlier studies, the phenomena required a long-lived coherence between the quantum states involved, and therefore were typically observed only at cryogenic temperatures. However, the characterization of an incoherent charge transfer between quantum wells (i.e., an inelastic tunneling current, which can occur at room temperature) has not previously been reported.

Here we describe the observation of room-temperature terahertz emission arising from the one-way (not oscillatory) tunneling current due to charge transfer

[*] markus.stein@physik.uni-marburg.de

© 2020 American Physical Society

between adjacent quantum wells. In contrast to earlier studies, which required an external bias to observe terahertz emission from quantum-well structures with a type-I band alignment [17,18], we use pairs of quantum wells that are arranged as a type-II structure. In these III-V ternary heterostructures, the band alignment is such that the energetically-most-favorable states for electrons in the conduction band and holes in the valence band are in opposite quantum wells; subsequently, after optical excitation of one quantum well, either the electron or the hole can find it energetically favorable to transfer via quantum tunneling to the opposite well, without applied bias. We demonstrate that this ultrafast inelastic charge transfer on length scales of a few nanometers produces a terahertz pulse. By selective modifications in the tunnel barrier of our model system, we unambiguously correlate the terahertz emission spectrum with the altered charge-transfer dynamics. Using a simple phenomenological model that captures the essential physics, we are able to reproduce the salient features of the measured spectra and connect them with the underlying current dynamics. Our results show that terahertz emission is a valuable marker to quantify ultrafast current dynamics in buried quantum structures, even at room temperature.

II. SAMPLE DESIGN

We use two sets of samples with different type-II band alignments [see Fig. 1(a)]. In the first set (designated as samples e1, e2, and e3), the electrons can tunnel through an intermediate barrier, while the holes remain in the quantum well in which they were optically excited. These samples consist of five periods of $Ga_{1-x}In_xAs/GaAs/GaN_yAs_{1-y}$ layers, with indium concentrations of around 24% and nitrogen concentrations of around 5% to ensure a conduction-band minimum in the Ga(N, As) layer, as shown in Fig. 1(a) (left). These three samples have different thicknesses of the intermediate GaAs barrier. As confirmed by both transmission-electron-microscopy and high-resolution x-ray-diffraction measurements, the barrier thickness d_{GaAs} is 1.5 nm for sample e1, 4.0 nm for sample e2, and 6.0 nm for sample e3. In the other sample set (referred to as h1, h2, and h3), the electrons and holes can both tunnel after photoexcitation, as shown by the oppositely directed arrows in Fig. 1(a) (right). Here, these samples consist of 50 periods of $Ga_{1-x}In_xAs/GaAs/GaAs_{1-y}Sb_y$ layers, with the GaAs tunneling barrier fixed at 1.0 nm and an indium concentration of around 5%. The Sb concentration is varied, with values of 3% for sample h1, 5% for sample h2, and 7%

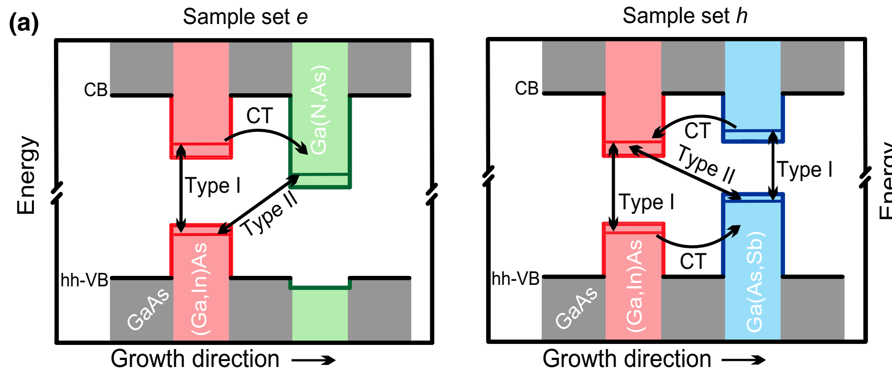

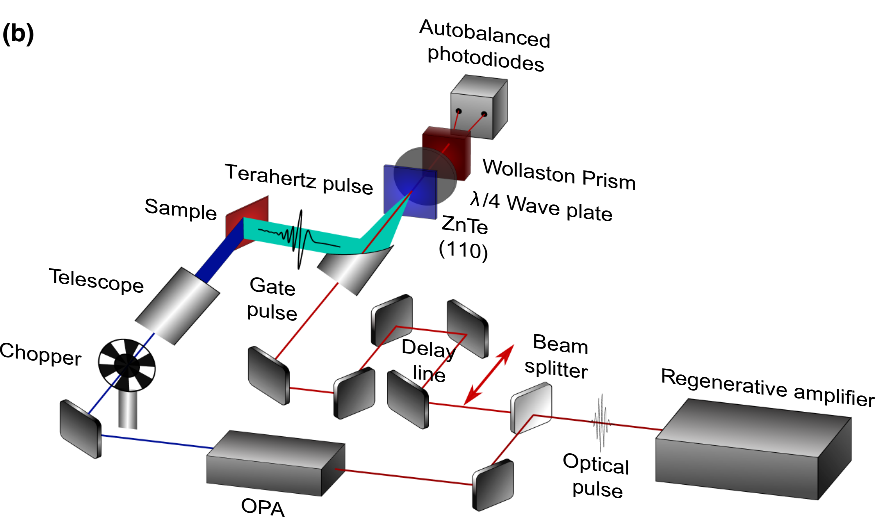

FIG. 1. (a) The band structure of the two sample series. Sample set e (e1, e2, and e3; left) allows the electrons to tunnel from the (Ga, In)As quantum wells into the Ga(N, As) quantum wells. In sample set h (h1, h2, and h3; right), either heavy-holes (hh) from the valence band (VB) of the (Ga, In)As quantum wells can tunnel into the Ga(As, Sb) quantum wells or electrons in the conduction band (CB) can tunnel in the opposite direction. The possible charge-transfer (CT) processes in both structures are marked with arrows. (b) Experimental setup. The terahertz path is flooded with dry nitrogen to remove water-vapor absorption signatures.

for sample h3. This tunes the band gap in the Ga(As, Sb) well between 1.35 and 1.40 eV, while the transition in the (Ga, In)As layer is fixed at 1.38 eV. This always ensures an energetically-most-favorable state for valence-band holes in the Ga(As, Sb) layer, while the conduction-band minimum is located in the (Ga, In)As layer. As a result, charge transfer and thus current flow after photoexcitation is oppositely directed in the two sample sets. In addition, we use two different samples as reference samples: a bare GaAs substrate and a typical type-I quantum-well sample, consisting of 50 periods of $Ga_{1-x}In_xAs$ quantum wells with an indium concentration of 10%. All samples are grown on (001) GaAs substrates by metalorganic vapor phase epitaxy (MOVPE). Details of the MOVPE growth procedure are outlined in Ref. [19] for the samples e1, e2, and e3 and in Ref. [20] for the samples h1, h2, and h3.

III. EXPERIMENTAL SETUP

The experimental setup is shown in Fig. 1(b). We use a Ti:sapphire regenerative-amplifier system, with a pulse energy of 5 mJ, a temporal duration (FWHM) of 35 fs, and a repetition rate of 1 kHz. A fraction of this beam pumps an optical parametric amplifier (OPA) to produce tunable output pulses. This collimated beam impinges on the sample at an incident angle of approximately 45°, with a spot size of approximately 4.5 mm. The pulse energy of the incident beam ranges from 0.12 to 10.8 μJ. After optical excitation of the sample, the emitted terahertz pulse in the specular direction is guided via an off-axis parabolic mirror to an 800-μm-thick ZnTe crystal for free-space electro-optic detection. The ZnTe crystal is positioned outside of the terahertz focus at a FWHM of the field of approximately 1.3 mm. As the detection crystal is moved from this position onwards away from the focus, the measured spectra no longer change significantly, so we can assume a frequency-independent (not a diffraction-limited) spot size. We emphasize that, unlike earlier measurements of terahertz emission from quantum wells, all our measurements are performed with the sample at room temperature.

IV. RESULTS AND DISCUSSION

We first consider the variation of the emitted terahertz signal with the wavelength of the incident femtosecond pulse. Figure 2(a) shows the detected terahertz waveforms obtained from sample h3 for different photon energies compared with the two reference samples. If the spectrally broad excitation pulse is centered at 1.34 eV, a good fraction of the pulse excites the direct 1s transition in the Ga(As, Sb) quantum well. The subsequent transfer of electrons to the (Ga, In)As quantum well, which occurs on a timescale of roughly 200 fs (inferred from optical-pump–white-light-probe data), leads to a short current pulse that is the source of the emitted terahertz pulse. If the wavelength is blueshifted to 1.38 eV, the overlap with optical transitions in the Ga(As, Sb) and (Ga, In)As quantum wells increases, resulting in a terahertz pulse with a slightly higher amplitude. A further blueshift to 1.46 eV leads only to a minute additional increase (not shown here). In this

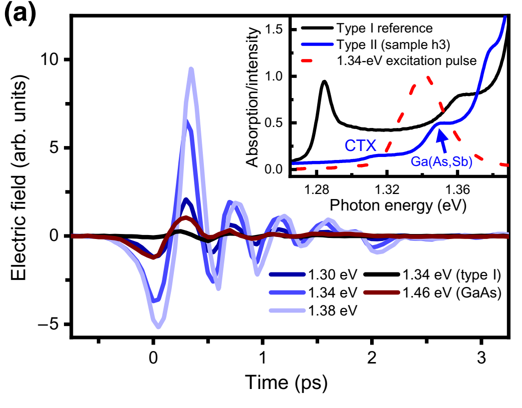

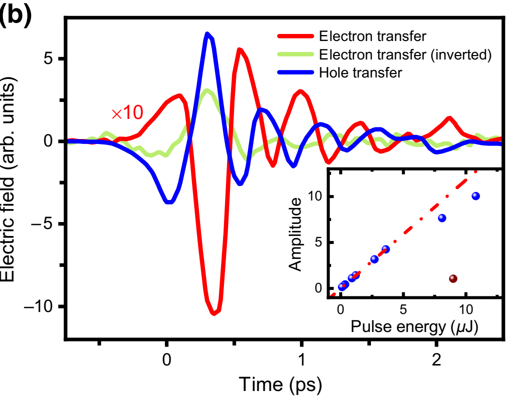

FIG. 2. (a) The emitted terahertz pulses from sample h3 for different photon energies of the excitation pulse. Also shown is the terahertz radiation from a bare GaAs surface emitter (brown line) as well as a conventional (Ga, In)As quantum-well reference sample (black line). The inset shows the linear absorption of the type-I reference sample and of sample h3, which features a type-II band alignment, along with the spectrum of an optical excitation pulse (dashed red line). (b) The emitted terahertz pulse of sample e1, which allows only electron transfer, is shown for a geometry where the quantum-well heterostructure is on top of the GaAs substrate (red line) and for an inverted sample (green line) where the optical excitation pulse has to pass through the substrate first. In addition, a typical terahertz pulse from the h1, h2, and h3 sample set (blue line) is shown; this generates a tunnel current in the opposite direction to that in the e1, e2, and e3 sample set. Both pulses from sample e1 are multiplied by a factor of 10 to take into account the 10-fold lower number of quantum wells compared with the h1, h2, and h3 sample set. The inset displays the maximum amplitude of the terahertz pulses of sample h3 (blue) for different pulse energies of the excitation at 1.36 eV. The maximum terahertz-pulse amplitude of a bare GaAs surface emitter (brown) excited at 1.46 eV is almost an order of magnitude smaller.

case the GaAs substrate is also excited. However, the emission from a bare GaAs substrate, which is caused by the photo-Dember effect [21], is roughly an order of magnitude weaker than the emission of the type-II heterostructure. In addition, the emission from the type-I quantum-well-heterostructure reference is almost another order of magnitude weaker when it is excited below the absorption edge of the GaAs substrate (e.g., at 1.34 eV). Therefore, we conclude that other previously studied effects [22–24] that may contribute to terahertz emission in quantum-well structures such as injection, shift, or light-induced drift currents or light-hole–heavy-hole beats are negligible. If the central pulse wavelength is redshifted, then the overlap with the direct transitions in the type-II heterostructure is reduced. This reduces the number of excited charge carriers, which reduces the current and thus the amplitude of the emitted terahertz pulse. Simultaneously, however, the spectral overlap with the resonance of the charge-transfer exciton [the peak at 1.31 eV in the inset in Fig. 2(a), labeled as CTX] increases. This transition has a much smaller oscillator strength than the direct transition of the Ga(As, Sb) and (Ga, In)As quantum wells, so only a small fraction of the optical pulse excites spatially indirect transitions. These constitute an instantaneous polarization in the material due to the spatially indirect nature of the transition. This optically driven polarization is able to produce a measurable terahertz signal, which could contribute to part of the measured signal at 1.30 eV. Yet, the strong increase of the signal when the excitation is shifted toward the type-I resonances (in the type-II samples), combined with the very weak signal obtained from the type-I reference sample, implies that the observed signal at 1.34 eV is dominated by the charge transfer between the two wells after photoexcitation.

To further verify that the terahertz emission originates from real-space charge transfer, we perform two checks. First, we flip the sample around, so that the excitation pulse is incident on the back surface rather than the front surface. As expected, this flips the polarity of the emitted terahertz signal [green curve in Fig. 2(b)], since the current flow is oppositely directed with respect to the direction of terahertz emission. Furthermore, it results in an additional delay of about 13 ps due to the extra propagation time for the optical and terahertz signals through the 500-μm-thick GaAs substrate. For better comparison of the terahertz waveforms with each other, the green curve in Fig. 2(b) is corrected by this delay. As a second test, we compare the terahertz signals from the h1, h2, and h3 sample set with those generated from the e1, e2, and e3 sample set, in which the charge transfer is oppositely directed. Again, we observe a flip of the polarity of the terahertz pulse, as expected [blue curve in Fig. 2(b)]. We also note that the signal is about a factor of 10 weaker, since samples e1, e2, and e3 contain only five periods of the double-quantum-well structure, rather than the 50 periods in the h1, h2, and h3 sample set. These results are all consistent with the idea that the terahertz signals originate from the charge-transfer process between adjacent quantum wells after photoexcitation. Since the emitted terahertz signal of the charge transfer scales with the number of quantum wells and with the energy of the excitation pulse [see the inset in Fig. 2(b)], similar type-II structures may also have the potential to operate as versatile room-temperature terahertz emitters.

We next investigate the dependence of the signal on the width of the barrier between the two quantum wells. The first set of samples (e1, e2, e3) are identical except for the barrier width. A thinner barrier should lead to a faster charge transfer, and therefore to a larger bandwidth of the emitted terahertz pulse. Optical-pump–optical-probe measurements on these samples under the same excitation conditions (see Appendix E) yield time constants associated with the charge-transfer process that range from 160 fs (for the thinnest barrier) to 13.3 ps (for the thickest one) at room temperature. As noted above, these times do not necessarily reflect solely the charge-transfer time, since those measurements are also sensitive to intrawell relaxation processes and other many-body effects [6,25]. However, they do provide an estimate of the rough timescales for the charge-transfer process. In Fig. 3, we show the terahertz emission spectra from the samples e1, e2, and e3,

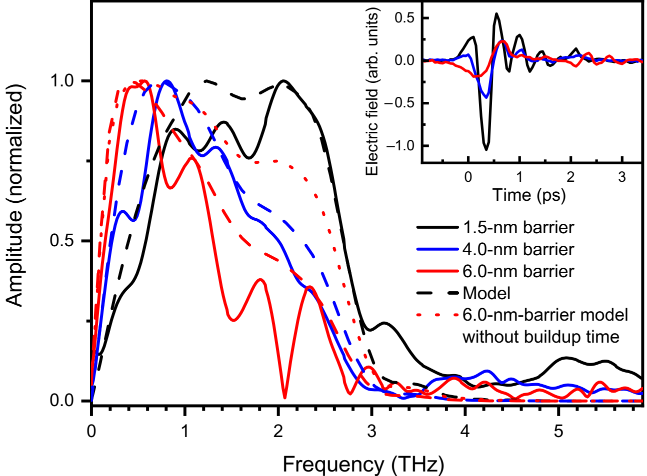

FIG. 3. Terahertz emission spectra for the three different barrier thicknesses in the e1, e2, and e3, sample set of 1.5 nm (solid black line), 4.0 nm (solid blue line), and 6.0 nm (solid red line). Also shown are the results of a phenomenological model that describes the barrier-thickness-dependent spectra using transfer times of 40 fs (dashed black line), 400 fs (dashed blue line), and 1.6 ps (dashed red line). The dotted red line is the result of the phenomenological model with a transfer time of 1.6 ps but without a time constant for the buildup of a tunnel current. The inset shows the measured time-domain terahertz pulses corresponding to the experimental spectra.

showing a clear correlation between barrier thickness and the bandwidth of the signals. As the barrier thickness increases, both the high-frequency edge and the low-frequency edge of the spectra shift to lower frequencies. This result is not consistent with an alternative explanation involving terahertz emission from the instantaneous polarization created by direct excitation of the charge-transfer exciton.

To understand these spectral changes, we develop a simple phenomenological model (details are given in Appendix D), in which the signal originates purely from the current (real-space charge transfer) between adjacent quantum wells. This calculation accounts for the duration of the Gaussian excitation pulse, and includes only two additional parameters: a time constant describing the exponential increase of the current after photoexcitation, and a second time constant describing the exponential decay of this current. For the former we use $t_{\text{buildup}} = 170$ fs as a constant value for all samples. Such a buildup time of the tunnel current is mandatory to describe the emission spectra. If the tunnel current sets in instantaneously with the optical excitation, the rise of the current would occur on the timescale of the 90-fs short excitation pulse. The result is a large bandwidth of the emitted terahertz pulse even for thickest barriers, as revealed by our phenomenological model (see Fig. 3). However, this is not consistent with our observations. Our results strongly suggest that incoherent tunnel currents do not start immediately but have to build up first. The time constant of this buildup is consistent with the observed buildup of a collective response of the many-body system and conductivity after photoexcitation in earlier reports [26,27]. Thus, we are able to monitor the lowest time limit for the onset of an incoherent current in the respective material. The second time constant ($t_{\text{tunneling}}$) describes the barrier-width-dependent tunneling time, for which we use $t_{e1} = 40$ fs, $t_{e2} = 400$ fs, and $t_{e3} = 1.6$ ps. As expected, these values are similar, but not identical, to the time constants we measure in optical-pump–optical-probe studies [6,25] (see Appendix E). From the modeled current transients, we compute a prediction for the terahertz waveform. We then use a spectral filter (the same for all three signals) that represents the response function of the thin (2-mm) Teflon beam block [28] and the 800-μm-thick ZnTe crystal used for terahertz detection [29]. The resulting curves reasonably accurately reproduce the measured spectra, including, in particular, the shifts of both the low-frequency and the high-frequency edges of the spectrum with barrier thickness.

For the thinnest barrier (sample e1), the high-frequency edge of the spectrum, which drops fairly sharply at about 2.5 THz, is determined by the spectral response of our ZnTe sensor, not by the charge-transfer dynamics. To capture the full bandwidth of the emitted terahertz pulse in a sample with faster dynamics, one can use a thinner detection crystal. To demonstrate this, we remeasure the signal from sample h3 using a 200-μm-thick GaP crystal, which has a broader spectral response. Figure 4 shows this experimental result (the respective time domain is shown in Appendix A) with the corresponding prediction based on the same model discussed above (but with use of the GaP detector response function [30,31], shown in Fig. 4). We observe that the model correctly forecasts the increase in the high-frequency content of the signal. Of course, a complete theoretical treatment of the problem would be much-more complex, including a fully-quantum-mechanical treatment of the tunneling process [32,33]. Nevertheless, these results establish that the narrowing of the spectrum in Fig. 3 reflects the slowing of the charge-transfer process for thicker barriers. The simple phenomenological model accurately captures the timescale of this process, which can be extracted easily from the measurements.

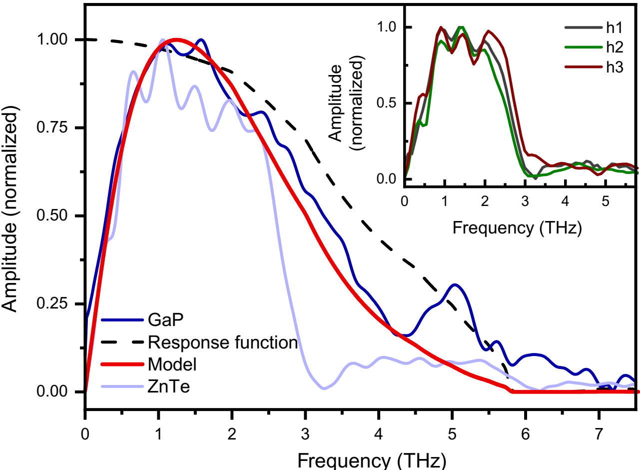

FIG. 4. Terahertz emission spectra for sample h3 for detection with an 800-μm-thick ZnTe crystal (light-blue line) and a 200-μm-thick GaP crystal (dark-blue line). The spectrum measured by the GaP crystal is described with the same phenomenological model (red line). The model includes a charge-transfer time of 60 fs for this sample. Also displayed is the response function (dashed black line) that accounts for the GaP detector response and the absorption of the Teflon beam block. The inset shows the normalized terahertz spectra of samples h1, h2, and h3, which all have the same nominal barrier thickness and differ only in their Sb concentrations.

Finally, we also measured the spectra of the terahertz emission from samples h1, h2, and h3, in which the band gap of the Ga(As, Sb) well varies but the barrier width is the same for all three samples. In this case, which is depicted in the inset in Fig. 4, we expect only small differences in the spectral width of the emission, due to the different relative populations of electrons [in the Ga(As, Sb) well] and holes [in the (Ga, In)As well] and their different transfer times. As anticipated, we find that these differences are small compared with the effect of changes in the tunneling barrier shown in Fig. 3. In addition, the measured

terahertz spectra and thus the charge-transfer times obtained are relatively insensitive to changes in excitation density and energy, as shown in Appendixes B and C.

V. SUMMARY

In summary, we characterize the incoherent charge transfer in a type-II quantum well using terahertz emission. This approach affords direct access to the photoinduced current arising from the tunneling process, without the confounding effects of carrier relaxation that often complicate the analysis of other measurements. Consequently, we observe that the terahertz emission spectra and thus the underlying charge-transfer dynamics are robust against a wide range of excitation conditions and are in our case almost exclusively determined by the thickness of the tunnel barrier. Furthermore, we easily observe an approximately-170-fs buildup dynamic of the tunneling process, since the phenomenological inclusion of this process is necessary to describe our data accurately. We also note that the surprisingly large terahertz signal, significantly larger than that observed from conventional methods of terahertz generation from bare semiconductor surfaces, offers an interesting possibility to design terahertz emitters through engineering of the type-II band structure and barrier width. Since the emission strength is scalable with the number of periods, this could lead to the development of powerful and spectrally agile terahertz sources.

ACKNOWLEDGMENTS

This work is a project of the Collaborative Research Center SFB 1083 funded by the Deutsche Forschungsgemeinschaft. In addition, D.M..M gratefully acknowledges the support of the Alexander von Humboldt Foundation.

APPENDIX A: DETECTION CRYSTALS

The terahertz emission of sample h3 is detected under the same excitation conditions of 4-μJ pulse energy at a central energy of 1.36 eV with two different crystals for electro-optic sampling. One is an 800-μm-thick ZnTe crystal and the other is a 200-μm-thick GaP crystal. The different detection bandwidths of the crystals result in different terahertz pulses in the time domain; these are shown in Fig. 5. It is evident that the detected terahertz pulse becomes shorter when the GaP crystal is used and approaches the expected waveform of a single zero crossing. In comparison, the pulse detected by ZnTe shows considerably more oscillations in the time domain, which are mainly caused by the lower detection bandwidth and the resulting spectral filtering of the terahertz pulse [34]. Here, the rather sharp cutoff edge of ZnTe near 2.5 THz leads to oscillations in its Fourier transform (i.e., the time domain).

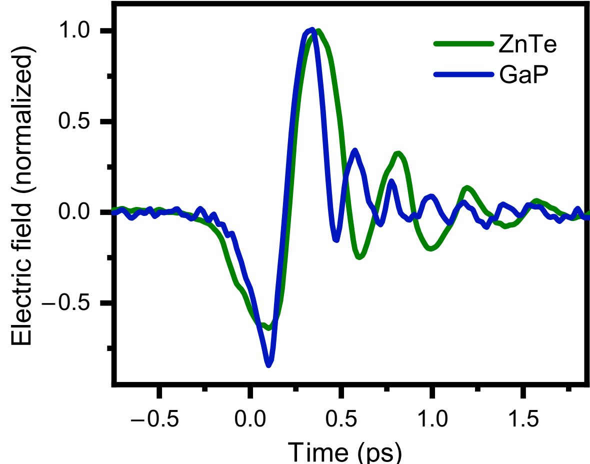

FIG. 5. The normalized terahertz pulse in the time domain as detected by an 800-μm-thick ZnTe crystal (green line) and a 200-μm-thick GaP crystal (line).

APPENDIX B: DEPENDENCE ON THE EXCITATION ENERGY

As stated in the main text, the terahertz emission results are very consistent for different excitation conditions. This is checked by examining sample h3 for different photon energies. The normalized terahertz emission spectra of sample h3 are shown in Fig. 6 for different excitation energies. The data show that the spectral response, especially for excitation energies between 1.27 and 1.34 eV, hardly changes. As a trend, the low-frequency components are represented somewhat more prominently in the spectrum for higher excitation energies. This is attributable to the fact that the (Ga, In)As quantum layers are excited to a greater extent at higher excitation energies. The hole tunneling from these quantum wells into the Ga(As, Sb) quantum wells is expected to be slower than the tunneling

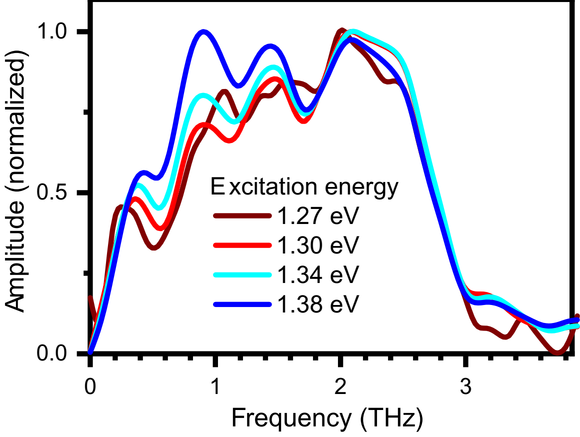

FIG. 6. The terahertz emission spectra of sample h3 for different photon energies of the excitation pulse.

of electrons in the reverse direction. As a consequence, the low-frequency components should be more pronounced in the spectrum, which corresponds perfectly with our observations. At a central photon energy of 1.38 eV, the GaAs substrate is already partially excited. This delays the filling of the quantum wells and thus further strengthens the low-frequency components in the spectrum.

APPENDIX C: DEPENDENCE ON THE EXCITATION DENSITY

The terahertz emission is also investigated as a function of the optical-pulse energy. The main text reveals that the maximum terahertz field strength increases almost linearly with the pulse energies investigated. As a complement, we show in Fig. 7 that the shape of the terahertz pulses in the time domain does not change for the different optical-pulse energies. Instead, only the field amplitude of the terahertz pulse increases with increasing pulse energy. This again underlines the reliability of terahertz emission results for different excitation conditions.

APPENDIX D: PHENOMENOLOGICAL MODEL

We apply a simple phenomenological model to describe the terahertz emission spectra. For this purpose, we assume that charge carriers $n(t)$ are excited by a Gaussian excitation pulse $g(t)$ via

$$n(t_i) = k \sum_{j=0}^{i} g(t_j)\Delta t_j,$$

where k is a constant factor and we use a Gaussian excitation pulse with a FWHM of 90 fs. This corresponds to the pulse length used in the experiment as confirmed by an autocorrelation measurement. Then we distinguish artificially between nontunneling states $n_{\mathrm{non}}(t)$ and conductive charge carriers $n_{\mathrm{con}}(t)$, where the former transform into the latter with a certain probability per time step p_1. Accordingly, the nontunneling states can easily be determined iteratively:

$$n_{\mathrm{non}}(t_{i+1}) = n_{\mathrm{non}}(t_i) + kg(t_{i+1})\Delta t_{i+1} - n_{\mathrm{non}}(t_i)p_1,$$

with

$$n_{\mathrm{non}}(t_0) = kg(t_0)\Delta t_0.$$

From the total number of excited charge carriers $n(t_i)$, the number of conductive charge carriers can thus be calculated via

$$n_{\mathrm{con}}(t_i) = n(t_i) - n_{\mathrm{non}}(t_i).$$

Conductive charge carriers can now contribute to a current by a tunneling process through the internal barrier. In our phenomenological model we assume that all charge carriers are generated in one quantum well and then tunnel through the barrier into the other quantum well with probability per time step p_2. This way we get the tunnel current $j(t)$:

$$j(t_{i+1}) = j(t_i) + \frac{\Delta n_{\mathrm{con}}(t_{i+1})}{\Delta t_{i+1}} - j(t_i)p_2,$$

with

$$j(t_0) = \frac{\Delta n_{\mathrm{con}}(t_0)}{\Delta t_0}.$$

The radiated terahertz field in the far field is proportional to the time derivative of the tunnel current $j(t)$ and can be converted into frequency space by Fourier transformation. For comparison with the experimental terahertz spectrum, the spectrum of the phenomenological model is finally multiplied by the detector response and the absorption of the Teflon beam block.

The exponential time constants t_{buildup} and $t_{\mathrm{tunneling}}$ given in the main text are derived from the probabilities per time unit p_1 and p_2 used for the iterative calculations. For p_1 we use a constant value of 0.005865 fs^{-1} for all samples, while p_2 ranges between 0.02469 and 0.000625 fs^{-1} depending on the barrier thickness.

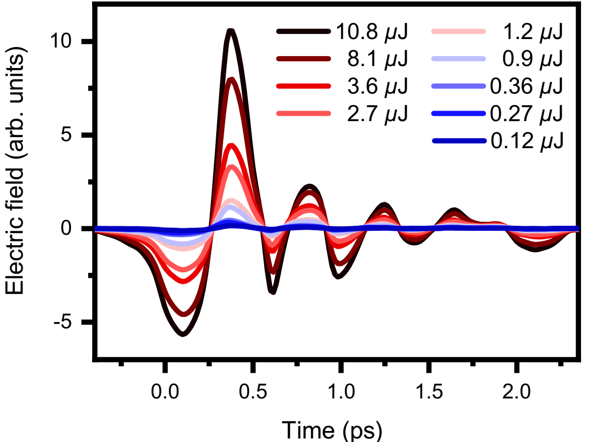

FIG. 7. The emitted terahertz pulses of sample h3 after excitation at 1.36 eV with different pulse energies.

APPENDIX E: OPTICAL-PUMP–OPTICAL-PROBE EXPERIMENTS

In addition to terahertz emission we perform optical-pump–optical-probe experiments under the same excitation conditions. Details of the optical-pump–optical-probe setup are given in Refs. [6,25]. Here we excite the samples at room temperature with a spot size of 4 mm and a pulse energy of 3.6 μJ at 1.34 eV, in analogy to the conditions in the terahertz emission experiments. To obtain the transients illustrated in Fig. 8, we integrate the spectrum over the respective excitonic resonance of the spatially

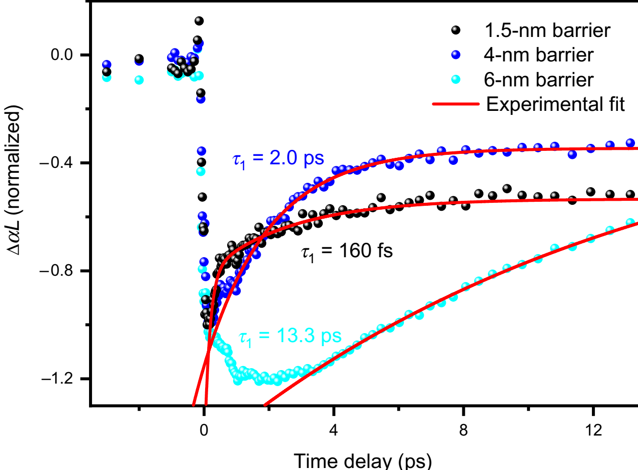

FIG. 8. Optical-pump–optical-probe transients of the excitonic resonances of the (Ga, In)As quantum wells in (Ga, InAs)/GaAs/Ga(N, As) heterostructures (e1, e2, and e3 sample set) with different inner GaAs barriers of different thicknesses.

direct transition as described in Ref. [6]. With the optical excitation, a bleaching signature of the excitonic resonance appears in all samples, independently of the respective barrier thickness. Subsequently, the signal recovers fastest for the thinnest inner barrier of 1.5 nm with a time constant of about 160 fs. This recovery of the bleaching signature is mainly driven by the charge-carrier transfer into the adjacent quantum well. As a result, it is in good agreement with the times obtained by our phenomenological model from the terahertz emission experiments for the buildup of the tunnel current and the tunneling process itself. We do not observe any temporal oscillations in our optical-pump–optical-probe data; therefore, we conclude that this is a one-way and not an oscillating tunneling process. For a thicker barrier of 4 nm, we observe a much-slower recovery of the bleaching signature in the optical-pump–optical-probe experiments on a timescale of 2 ps. For the thickest barrier of 6 nm, the bleaching signature increases first after optical excitation. Here, relaxation processes probably dominate the bleaching signature initially compared with the comparatively slow charge-carrier transfer. These relaxation processes on a picosecond timescale of course also affect the signatures of samples with other barrier thicknesses. However, because of the dominant influence of the charge transfer on these timescales, other processes are not visible in the measured data in the case of thinner barriers. Nevertheless, those other interactions of the many-particle system obviously affect the dynamics of optical-pump–optical-probe experiments in the first few picoseconds. Accordingly, it is very difficult to derive the actual charge-transfer dynamics with those optical experiments. A comparison with our terahertz emission indicates that the differences between both methods increase with increasing transfer times of the charge carriers.

[1] J. Faist, F. Capasso, D. L. Sivco, C. Sirtori, A. L. Hutchinson, and A. Y. Cho, Quantum cascade laser, Science **264**, 553 (1994).
[2] B. S. Williams, Terahertz quantum-cascade lasers, Nat. Photonics **1**, 517 (2007).
[3] J. Feldmann, R. Sattmann, E. O. Göbel, J. Kuhl, J. Hebling, K. Ploog, R. Muralidharan, P. Dawson, and C. T. Foxon, Subpicosecond Real-Space Charge Transfer in Type-II GaAs/AlAs Superlattices, Phys. Rev. Lett. **62**, 1892 (1989).
[4] G. Livescu, A. M. Fox, D. A. B. Miller, T. Sizer, W. H. Knox, A. C. Gossard, and J. H. English, Resonantly Enhanced Electron Tunneling Rates in Quantum Wells, Phys. Rev. Lett. **63**, 438 (1989).
[5] J. Feldmann, J. Nunnenkamp, G. Peter, E. Göbel, J. Kuhl, K. Ploog, P. Dawson, and C. T. Foxon, Experimental study of the Γ-X electron transfer in type-II (Al, Ga)As/AlAs superlattices and multiple-quantum-well structures, Phys. Rev. B **42**, 5809 (1990).
[6] M. Stein, C. Lammers, M. J. Drexler, C. Fuchs, W. Stolz, and M. Koch, Enhanced Absorption by Linewidth Narrowing in Optically Excited Type-II Semiconductor Heterostructures, Phys. Rev. Lett. **121**, 017401 (2018).
[7] T. Tada, A. Yamaguchi, T. Ninomiya, H. Uchiki, T. Kobayashi, and T. Yao, Tunneling process in AlAs/GaAs double quantum wells studied by photoluminescence, J. Appl. Phys. **63**, 5491 (1988).
[8] T. B. Norris, N. Vodjdani, B. Vinter, C. Weisbuch, and G. A. Mourou, Charge-transfer-state photoluminescence in asymmetric coupled quantum wells, Phys. Rev. B **40**, 1392 (1989).
[9] M. G. W. Alexander, M. Nido, W. W. Rühle, and K. Köhler, Resonant-tunneling transfer times between asymmetric GaAs/$Al_{0.35}Ga_{0.65}$As double quantum wells, Phys. Rev. B **41**, 12295 (1990).
[10] S. Schmitt-Rink, D. S. Chemla, and D. A. B. Miller, Theory of transient excitonic optical nonlinearities in semiconductor quantum-well structures, Phys. Rev. B **32**, 6601 (1985).
[11] M. Kira, F. Jahnke, and S. W. Koch, Microscopic Theory of Excitonic Signatures in Semiconductor Photoluminescence, Phys. Rev. Lett. **81**, 3263 (1998).
[12] K. Hannewald, S. Glutsch, and F. Bechstedt, Theory of photoluminescence in semiconductors, Phys. Rev. B **62**, 4519 (2000).
[13] M. C. Beard, G. M. Turner, and C. A. Schmuttenmaer, Measuring intramolecular charge transfer via coherent generation of THz radiation, J. Phys. Chem. A **106**, 878 (2002).
[14] H. Zhan, J. Deibel, J. Laib, C. Sun, J. Kono, D. M. Mittleman, and H. Munekata, Temperature dependence of terahertz emission from InMnAs, Appl. Phys. Lett. **90**, 012103 (2007).
[15] T. Seifert, et al., Efficient metallic spintronic emitters of ultrabroadband terahertz radiation, Nat. Photonics **10**, 483 (2016).
[16] E. Y. Ma, B. Guzelturk, G. Li, L. Cao, Z.-X. Shen, A. M. Lindenberg, and T. F. Heinz, Recording interfacial currents on the subnanometer length and femtosecond time scale by terahertz emission, Sci. Adv. **5**, eaau0073 (2019).
[17] C. Waschke, H. G. Roskos, R. Schwedler, K. Leo, H. Kurz, and K. Köhler, Coherent Submillimeter-Wave Emission

From Bloch Oscillations in a Semiconductor Superlattice, Phys. Rev. Lett. **70**, 3319 (1993).

[18] M. C. Nuss, P. C. M. Planken, I. Brener, H. G. Roskos, M. S. C. Luo, and S. L. Chuang, Terahertz electromagnetic radiation from quantum wells, Appl. Phys. B **58**, 249 (1994).

[19] C. Schlichenmaier, H. Grüning, A. Thränhardt, P. J. Klar, B. Kunert, K. Volz, W. Stolz, W. Heimbrodt, T. Meier, and S. W. Koch, Type I-type II transition in InGaAs–GaNAs heterostructures, Appl. Phys. Lett. **86**, 081903 (2005).

[20] C. Fuchs, A. Beyer, K. Volz, and W. Stolz, MOVPE growth of (GaIn) As/Ga (AsSb)/(GaIn) As type-II heterostructures on GaAs substrate for near infrared laser applications, J. Cryst. Growth **464**, 201 (2017).

[21] J. N. Heyman, N. Coates, A. Reinhardt, and G. Strasser, Diffusion and drift in terahertz emission at GaAs surfaces, Appl. Phys. Lett. **83**, 5476 (2003).

[22] P. C. M. Planken, M. C. Nuss, I. Brener, K. W. Goossen, M. S. C. Luo, S. L. Chuang, and L. Pfeiffer, Terahertz Emission in Single Quantum Wells After Coherent Optical Excitation of Light Hole and Heavy Hole Excitons, Phys. Rev. Lett. **69**, 3800 (1992).

[23] M. Bieler, K. Pierz, and U. Siegner, Simultaneous generation of shift and injection currents in (110)-grown GaAsâĹŢAlGaAs quantum wells, J. Appl. Phys. **100**, 083710 (2006).

[24] J. Maysonnave, S. Huppert, F. Wang, S. Maero, C. Berger, W. de Heer, T. B. Norris, L. A. De Vaulchier, S. Dhillon, J. Tignon, R. Ferreira, and J. Mangeney, Terahertz generation by dynamical photon drag effect in graphene excited by femtosecond optical pulses, Nano Lett. **14**, 5797 (2014).

[25] L. Rost, S. Gies, M. Stein, C. Fuchs, S. Nau, P. Kükelhan, K. Volz, W. Stolz, M. Koch, and W. Heimbrodt, Correlation of optical properties and interface morphology in type-II semiconductor heterostructures, J. Phys.: Condens. Matter **31**, 014001 (2019).

[26] R. Huber, F. Tauser, A. Brodschelm, M. Bichler, G. Abstreiter, and A. Leitenstorfer, How many-particle interactions develop after ultrafast excitation of an electron–hole plasma, Nature **414**, 286 (2001).

[27] D. Turchinovich, F. D'Angelo, and M. Bonn, Femtosecond-timescale buildup of electron mobility in GaAs observed via ultrabroadband transient terahertz spectroscopy, Appl. Phys. Lett. **110**, 121102 (2017).

[28] P. D. Cunningham, N. N. Valdes, F. A. Vallejo, L. M. Hayden, B. Polishak, X.-H. Zhou, J. Luo, A. K.-Y. Jen, J. C. Williams, and R. J. Twieg, Broadband terahertz characterization of the refractive index and absorption of some important polymeric and organic electro-optic materials, J. Appl. Phys. **109**, 043505 (2011).

[29] A. Leitenstorfer, S. Hunsche, J. Shah, M. C. Nuss, and W. H. Knox, Detectors and sources for ultrabroadband electro-optic sampling: Experiment and theory, Appl. Phys. Lett. **74**, 1516 (1999).

[30] Q. Wu and X.-C. Zhang, 7 terahertz broadband GaP electro-optic sensor, Appl. Phys. Lett. **70**, 1784 (1997).

[31] B. Wu, L. Cao, Q. Fu, P. Tan, and Y. Xiong, in *Proceedings of the 5th International Particle Accelerator Conference* (2014), p. 2891.

[32] H. Vaupel, P. Thomas, O. Kühn, V. May, K. Maschke, A. P. Heberle, W. W. Rühle, and K. Köhler, Dissipative tunneling in asymmetric double-quantum-well systems: A coherence phenomenon, Phys. Rev. B **53**, 16531 (1996).

[33] O. Schubert, M. Hohenleutner, F. Langer, B. Urbanek, C. Lange, U. Huttner, D. Golde, T. Meier, M. Kira, S. W. Koch, and R. Huber, Sub-cycle control of terahertz high-harmonic generation by dynamical Bloch oscillations, Nat. Photonics **8**, 119 (2014).

[34] H. J. Bakker, G. C. Cho, H. Kurz, Q. Wu, and X.-C. Zhang, Distortion of terahertz pulses in electro-optic sampling, J. Opt. Soc. Am. B **15**, 1795 (1998).